Les Cahiers du GERAD ISSN: 0711–2440

Updating simulated multi-attribute orebody models using high-order statistics considering production data of multiple support scales

L. Findlay, R. Dimitrakopoulos

G–2025–59

September 2025

La publication de ces rapports de recherche est rendue possible grâce au soutien de HEC Montréal, Polytechnique Montréal, Université McGill, Université du Québec à Montréal, ainsi que du Fonds de recherche du Québec – Nature et technologies.

Dépôt légal – Bibliothèque et Archives nationales du Québec, 2025
– Bibliothèque et Archives Canada, 2025

The publication of these research reports is made possible thanks to the support of HEC Montréal, Polytechnique Montréal, McGill University, Université du Québec à Montréal, as well as the Fonds de recherche du Québec – Nature et technologies.

Legal deposit – Bibliothèque et Archives nationales du Québec, 2025
– Library and Archives Canada, 2025

GERAD HEC Montréal
3000, chemin de la Côte-Sainte-Catherine
Montréal (Québec) Canada H3T 2A7

Tél. : 514 340-6053
Téléc. : 514 340-5665
info@gerad.ca
www.gerad.ca

Updating simulated multi-attribute orebody models using high-order statistics considering production data of multiple support scales

Liam Findlay [a, b]

Roussos Dimitrakopoulos [a, b]

[a] *COSMO – Stochastic Mine Planning Laboratory Department of Mining and Materials Engineering, McGill University, Montréal (Qc), Canada, H3A 0E8*

[b] *GERAD, Montréal (Qc), Canada, H3T 1J4*

liam.findlay@mail.mcgill.ca
roussos.dimitrakopoulos@mcgill.ca

September 2025
Les Cahiers du GERAD
G–2025–59

Abstract : Operating mining complexes constantly collect data from a wide variety of sources that directly or indirectly measure pertinent geological and geometallurgical attributes of mined material. These attributes are critical to processing performance and the quality of sellable products. Thus, integrating new information to rapidly update simulated orebody models of these attributes facilitates adaptive decision-making within the context of stochastic optimization for short-term production planning. The proposed framework updates multiple correlated attributes of simulated orebody block models given production data of two types. The first includes spatial measurements at point support scale such as blasthole assays or drill penetration rates. The second type includes processing performance measurements such as mill throughput or metal recovery which depend on the properties of blended materials. The measurements are used as additional conditioning data to construct posterior probability distributions for attributes of nearby blocks. Within a block, values for multiple attributes are updated sequentially, with each attribute being used to condition the next. The high-order updating framework reproduces complex geological patterns and does not make any assumptions on the underlying distributions. A case study using a multi-element iron deposit illustrates the performance of the updating framework.

Keywords : Geostatistical simulation; data assimilation; high-order spatial statistics; stochastic orebody modelling; mining complex

---

Acknowledgements: The work in this paper was funded by The National Sciences and Engineering Research Council (NSERC) of Canada CRD Grant 500414- 16 and NSERC Discovery Grant 239019, the industry consortium members of McGill University's COSMO Stochastic Mine Planning Laboratory [AngloGold Ashanti, Agnico Eagle, BHP, De Beers, AngloAmerican, IAMGOLD, Kinross Gold, Newmont Mining, and Vale]; and the Canada Research Chairs Program.

Conflict of Interest The authors declare that they have no financial or non-financial conflict of interest related to the content of this manuscript.

1 Introduction

The performance of an industrial mining complex that extracts, transports, and processes materials to create valuable mineral products depends on the properties of the raw materials (Goodfellow and Dimitrakopoulos 2016, 2017; Montiel and Dimitrakopoulos 2018; Dimitrakopoulos and Lamghari 2022; Both and Dimitrakopoulos 2023). At the time of long-term planning, the quality and spatial distributions of important material properties such as rock types, metal grades, or geometallurgical attributes are uncertain due to the sparse nature of exploration measurements (Dimitrakopoulos et al. 2002; Dowd 1997). However, a significant amount of data can be collected during production that provides more information describing the material in the ground. Using this additional data to update simulated orebody models of the deposit allows for short-term planning decisions to be made with the most recently updated information, ultimately leading to an adaptive optimization of the mining complex (Benndorf 2015, 2020; Kumar et al. 2020; de Carvalho and Dimitrakopoulos 2023). The critical aspect that enables adaptive decision making is the use of measurements taken from mined materials to update properties of nearby materials that may be extracted in the near future.

Data can be collected from a wide variety of sources throughout a mining complex, with each source having its own capabilities and precision which need to be accounted for. Blasthole drilling can provide measurements when samples are assayed for metal grades (Rossi and Deutsch 2014) and drilling performance can indicate rock hardness (Vezhapparambu et al. 2018). Contactless sensors such as infrared and X-ray scanners can measure metal properties from materials passing through a conveyor belt (Robben and Wotruba 2019). Numerous measurements of processing performance such as grinding throughput, screen separation quantities, reagent consumption, or metal recovery can be recorded during material processing. These performance measurements depend on geometallurgical properties of the feed and should be used to update the same relevant properties of in situ material. While data from blasthole drilling inherently includes spatial coordinates, measurements taken downstream on blended materials need to be referenced back to their original in situ locations. Several technological advances have made tracking material through a mining complex possible. La Rosa et al. (2018) deployed radiofrequency identification tags in an underground mine to track material and better link plant performance with lab data from material samples. Chaowasakoo et al. (2014) use GPS data to track the movement of mobile equipment in an open pit mine. Several researchers have relied on these technologies to connect mill throughput data to in situ material locations (Wambeke et al. 2018; Both and Dimitrakopoulos 2022). Operations that cannot accurately track material will be unable to use downstream processing data to update orebody models. In addition, even if the original locations of processed materials can be identified, downstream measurements taken on blended feed must be associated with all locations, as it is not possible to isolate the contribution of each individual mining unit. An updating approach that aims to use all this data must be able to simultaneously analyze multiple support scales (point, block, and blended production feed) and produce a single posterior distribution for relevant material properties. Geostatistical techniques have been used to integrate new data into spatial models with early development focusing on linear estimation methods such as kriging or cokriging (Kitanidis and Vomvoris 1983; Vargas-Guzmán and Yeh 1999). In the field of petroleum reservoir management, other methods have been developed under the name of history matching (Oliver and Chen 2011). In mining applications, conditional simulation of successive residuals (Vargas-Guzmán and Dimitrakopoulos 2002; Jewbali and Dimitrakopoulos 2011) has been developed to update simulations for mineral deposits within the framework of LU simulation. More recent mining applications have applied the Ensemble Kalman Filter (EnKF) (Evensen 1994, 2003) to update orebody simulations(Benndorf 2015; Yüksel et al. 2016; Wambeke and Benndorf 2017; Wambeke et al. 2018; Benndorf 2020; Kumar et al. 2020; de Carvalho and Dimitrakopoulos 2023). Like the previously mentioned approaches, the EnKF method assumes that the underlying random field representing the mineral deposit follows a multi-Gaussian distribution. It makes the same assumption for the multivariate distribution connecting the random field and the observations used for updating. With these assumptions, it can use a covariance model to capture the two-point spatial statistics of available data.

In reality, attributes in mineral deposits do not follow Gaussian distributions and two-point statistics fail to capture complex spatial patterns or the connectivity of extreme values.

High-order spatial statistics are able to capture complex patterns and high-order simulation algorithms use these statistics to simulate orebody models without assuming underlying distributions (Dimitrakopoulos et al. 2010; Mustapha and Dimitrakopoulos 2010, 2011; Minniakhmetov et al. 2018; Yao et al. 2018; de Carvalho et al. 2019; Dimitrakopoulos and Yao 2022). Kumar and Dimitrakopoulos (2022) developed a method to update high-order simulations from new information using a reinforcement learning agent that is rewarded for reproducing the high-order spatial statistics of available data. However, the approach only updates point values which is less efficient than directly updating block values. In addition, it only considers a single material attribute, and its reward signal calculates conditional probabilities given each data type separately, ignoring the correlations between them.

The framework proposed in this work updates orebody simulations directly at block support by constructing conditional probability distributions of the block values given the production measurements available. The distributions are built without assuming the distribution's shape by using orthogonal polynomials with coefficients inferred from the high-order spatial statistics of training image (TI) data. The TI should be a geological analog for the mining area such as a previously mined section from the same deposit. The distributions are then sampled to obtain the updated values, maintaining the integrity of each distribution rather than only keeping the expected or maximum likelihood value. Multiple correlated block attributes are updated in a joint sequential simulation procedure. Nearby data from all available sources including production measurements taken at point support and initial simulated values at block support are included in a single set of conditioning data to capture all correlations. Any measurement type is possible for conditioning if the TI includes the same data type. Downstream measurements from blended materials are assigned to all blocks that contributed to the measurement and used as additional conditioning data. While the approach cannot isolate each block's contribution to each measurement, assigning downstream measurements to spatial locations provides a way for these measurements to be used for updating blocks that have not yet been mined but are nearby to those that have. In the following section, a description and mathematical formulation of the updating method are given. Subsequently, a demonstration of the framework is presented using a multi-attribute iron ore deposit. Conclusions and future work are highlighted in the final section.

2 Method

This section describes the method used for the proposed updating framework by first formally defining the problem and its notation, then reviewing the method of distribution approximation with orthogonal polynomials, extending this method to account for multi-attribute block values, and finally outlining the procedure followed to execute the framework.

2.1 Updating block values with sequential simulation

Let $\mathbf{Z}=\left[Z^1,\ldots,Z^A\right]$ represent a block-support vector random field (RF) which consists of individual RFs corresponding to attributes $a \in \{1,\ldots,A\}$ defined at block locations $b_i \in \mathcal{D} \subseteq \mathcal{R}^n, i=1,\ldots,N_B$, where N_B is the number of blocks in the n-dimensional domain $\mathcal{D}$. The attributes $a \in \{1,\ldots,A\}$ represent in situ block properties such as metal grades, for example. An outcome of the random variable for block attribute a at location b_i is denoted using $z^a(b_i) = z_i^a$. Let $\mathbf{X}=\left[X^1,\ldots,X^R\right]$ represent a block-support vector RF with individual RFs corresponding to processing performance measurements $r \in \{1,\ldots,R\}$ defined at block locations $b_i \in \mathcal{D} \subseteq \mathcal{R}^n, i=1,\ldots,N_B$. Processing performance measurements $r \in \{1,\ldots,R\}$ are observed during production and allocated to the blocks that were blended and processed to yield them. Let $\mathbf{Y}=\left[Y^1,\ldots,Y^T\right]$ represent a point-support vector RF with individual RFs each corresponding to a spatial measurement $t \in \{1,\ldots,T\}$ and defined at point locations $p_j \in \mathcal{D} \subseteq \mathcal{R}^n, j=1,\ldots,N_P$ where N_P is the number of points in the same domain $\mathcal{D}$. An example of

point-support data is grade assays from blastholes. All RFs are assumed to be zero-mean, stationary, and ergodic.

$\Lambda = \left[x_1^1, \ldots, x_{N_P}^R, y_1^1, \ldots y_{N_P}^T\right]$ is used to refer to the entire set of production measurements and can be indexed by $\Lambda_d, d = 1, \ldots, N_D$ where $N_D = R \cdot N_B + T \cdot N_P$. Sometimes the abbreviated set notation $z_1^1, \ldots, z_i^a$ will appear. To clarify the meaning of both the subscript and superscript being incremented during the "…", it refers to a one-dimensional array containing all elements of a two-dimensional array defined by

$$z_1^1, \ldots, z_i^a = \begin{bmatrix} z_1^1 & \cdots & z_1^a \\ \vdots & \ddots & \vdots \\ z_i^1 & \cdots & z_i^a \end{bmatrix}. \tag{1}$$

The proposed approach aims to update the block attributes $\mathbf{Z}$ using the framework of sequential high-order stochastic simulation (Mustapha and Dimitrakopoulos 2011; Minniakhmetov et al. 2018; Yao et al. 2018; de Carvalho et al. 2019; Dimitrakopoulos and Yao 2022) while using the production measurements Λ as conditioning data. Sequential simulation allows reproduction of the conditional joint probability density function (pdf) based on a product of conditional univariate pdfs (Journel and Alabert 1989).

$$\begin{aligned} &f\left(z_1^1, \ldots, z_{N_B}^A | \Lambda\right) \\ &\quad = f\left(z_1^1 | \Lambda\right) \cdot f\left(z_1^2 | z_1^1, \Lambda\right) \cdot f\left(z_1^3 | z_1^1, z_1^2, \Lambda\right) \cdot \ldots \\ &\qquad \cdot f\left(z_{N_B}^A | z_1^1, \ldots, z_{N_B-1}^A, z_{N_B}^1, \ldots, z_{N_B}^{A-1}, \Lambda\right). \end{aligned} \tag{2}$$

Assuming z_i^a is the current block attribute being updated, then the conditional distribution can be expressed in terms of the joint distribution using Bayes' rule (Stuart and Ord 2004)

$$\begin{aligned} f\left(z_i^a | z_1^1, \ldots, z_{i-1}^A, z_i^1, \ldots, z_i^{a-1}, \Lambda\right) &= \frac{f\left(z_1^1, \ldots, z_{i-1}^A, z_i^1, \ldots, z_i^a, \Lambda\right)}{f\left(z_1^1, \ldots, z_{i-1}^A, z_i^1, \ldots, z_i^{a-1}, \Lambda\right)} \\ &= \frac{f\left(z_1^1, \ldots, z_{i-1}^A, z_i^1, \ldots, z_i^a, \Lambda\right)}{\int f\left(z_1^1, \ldots, z_{i-1}^A, z_i^1, \ldots, z_i^a, \Lambda\right) db_i}. \end{aligned} \tag{3}$$

Thus, the block values can be updated by approximating the joint pdf.

2.2 Approximating joint probability density functions

For now, consider a single random variable Z defined by the pdf $f(z)$ on the domain $[a, b]$ and let $\varphi_1(z), \varphi_2(z), \ldots$ be a complete system of orthogonal basis functions defined on the same space. Then $f(z)$ can be approximated by a finite number ω of these functions: $\varphi_1(z), \varphi_2(z), \ldots, \varphi_\omega(z)$, such that

$$f(z) \approx \sum_{m=0}^{\omega} L_m \varphi_m(z) \tag{4}$$

where L_m is the coefficient of approximation for the function of order m. Since the functions are orthogonal,

$$\int_a^b \varphi_m(z)\varphi_k(z)dz = \delta_{mk} \tag{5}$$

where δ_{ij} is the Kronecker delta such that $\delta_{mk} = \begin{cases} 1, & m = k \\ 0, & m \neq k. \end{cases}$ The coefficients can be derived from the expected values of the basis functions

$$\begin{aligned} \mathbb{E}\left[\varphi_k(z)\right] &= \int_a^b \varphi_k(z) f(z) dz \approx \int_a^b \varphi_k(z) \sum_{m=0}^{\omega} L_m \varphi_m(z) dz \\ &= \sum_{m=0}^{\omega} L_m \int_a^b \varphi_m(z)\varphi_k(z)dz = \sum_{m=0}^{\omega} L_m \delta_{mk} = L_k. \end{aligned} \tag{6}$$

Thus, the coefficients can be estimated from available data and used to construct the approximated pdf. The present work uses Legendre polynomials (Mustapha and Dimitrakopoulos 2010, 2011) as the orthogonal basis functions, but other functions such as Legendre-like splines (Minniakhmetov et al. 2018; de Carvalho et al. 2019) could be used as well.

2.3 Approximating joint probability density functions of a vector random field

Several studies (Mustapha and Dimitrakopoulos 2011; Minniakhmetov et al. 2018) demonstrate how the formulation above can be extended to approximate a joint pdf of a set of random variables in a random field. de Carvalho et al. (2019) show that the multivariate case can be applied to simulate block-support values using point-support conditioning data. Using the previously defined vector RF notation for block attributes, this section generalizes the same formulation to approximate joint pdfs of random variables which represent multiple block attributes and therefore do not all belong to a single RF. First, the joint pdf from Equation 3 is approximated using the same orthogonal basis functions

$$\begin{aligned} & f\left(z_1^1, \ldots z_{i-1}^A, z_i^1, \ldots, z_i^a, \Lambda\right) \\ & \quad \approx \sum_{m_1^1=0}^{\omega} \cdots \sum_{m_{i-1}^A=0}^{\omega} \sum_{m_i^1=0}^{\omega} \cdots \sum_{m_i^a=0}^{\omega} \sum_{\lambda_1=0}^{\omega} \cdots \sum_{\lambda_{N_D}=0}^{\omega} L_{m_1^1,\ldots,m_{i-1}^A,m_i^1,\ldots,m_i^a,\lambda_1,\ldots,\lambda_{N_D}} \cdot \varphi_{m_1^1}\left(z_1^1\right) \\ & \qquad \cdot \ldots \cdot \varphi_{m_{i-1}^A}\left(z_{i-1}^A\right) \cdot \varphi_{m_i^1}\left(z_i^1\right) \cdot \ldots \cdot \varphi_{m_i^a}\left(z_i^a\right) \cdot \varphi_{\lambda_1}\left(\Lambda_1\right) \cdot \ldots \cdot \varphi_{\lambda_{N_D}}\left(\Lambda_{N_D}\right). \end{aligned} \tag{7}$$

Next, the same derivation from Equation 6 is applied to relate the coefficients to the expected value of the product of basis functions (a full multivariate derivation is shown in the Appendix)

$$\begin{aligned} & \mathbb{E}\left[\varphi_{k_1^1}\left(z_1^1\right) \cdot \ldots \cdot \varphi_{k_{i-1}^A}\left(z_{i-1}^A\right) \cdot \varphi_{k_i^1}\left(z_i^1\right) \cdot \ldots \cdot \varphi_{k_i^a}\left(z_i^a\right) \cdot \varphi_{l_1}\left(\Lambda_1\right) \cdot \ldots \cdot \varphi_{l_{N_D}}\left(\Lambda_{N_D}\right)\right] \\ & \quad \approx L_{k_1^1,\ldots,k_{i-1}^A,k_i^1,\ldots,k_i^a,l_1,\ldots,l_{N_D}}. \end{aligned} \tag{8}$$

In practice, the data used to condition a given block is limited to a local neighbourhood with a configuration called the spatial template, τ. The approximation coefficients are estimated from training data replicates that match the same spatial template

$$\begin{aligned} & L_{k_1^1,\ldots,k_{i-1}^A,k_i^1,\ldots,k_i^a,l_1,\ldots,l_{N_D}} \\ & \quad \approx \frac{1}{M_\tau} \sum_{c=1}^{M_\tau} \varphi_{k_1^1}\left(z_1^1\right) \cdot \ldots \cdot \varphi_{k_{i-1}^A}\left(z_{i-1}^A\right) \cdot \varphi_{k_i^1}\left(z_i^1\right) \cdot \ldots \cdot \varphi_{k_i^a}\left(z_i^a\right) \\ & \qquad \cdot \varphi_{l_1}\left(\Lambda_1\right) \cdot \ldots \cdot \varphi_{l_{N_D}}\left(\Lambda_{N_D}\right) \end{aligned} \tag{9}$$

where M_τ is the number of replicates found matching τ. It is worth noting that because all attributes used in the conditioning data must be included in the calculation of coefficients, this approach requires training data for all attributes and measurement types to exist in a set of collocated training images. For example, an already mined-out area could be used if it includes a block model with all primary material attributes ($\mathbf{Z}$) as well as spatial measurements ($\mathbf{Y}$) and processing performance measurements assigned to blocks ($\mathbf{X}$).

2.4 Algorithm for updating block values

After operational data has been collected, the process can update block values for all material properties in each simulated orebody realization. Each realization is updated separately using the following procedure.

1. Define a path to visit each block in the simulation grid, starting with the blocks most recently mined and selecting other blocks randomly.

2. For the current block b_i, define a random sequence to update each attribute.
3. For the current attribute a, identify nearby conditioning data including production measurements Λ and nearby block values $\mathbf{Z}$, creating a spatial template τ.
4. Scan the TI for replicates matching the template τ.
5. Calculate Legendre coefficients with the replicates using Equation 9.
6. Construct the conditional pdf for z_i^a using Equations 7 and 3.
7. Sample the conditional pdf to obtain the updated value.
8. Return to step 3 for the next attribute or return to step 2 with the next block if all attributes for the current block have been updated.

3 Application with a multi-attribute iron ore deposit

A two-dimensional iron ore deposit with five attributes (iron, silica, alumina, phosphorus, and loss-on-ignition) is used to demonstrate the proposed method. A set of initial simulations for the five attributes $\left(\mathbf{Z}=\left[Z^1,\ldots,Z^5\right]\right)$ are generated using the joint high-order simulation method (Minniakhmetov and Dimitrakopoulos 2017) and converted to block support. A separately created realization is considered the "ground truth" model for each attribute.

Several sources of synthetically created production measurements are used for updating the simulations. Spatial data sources include point-support measurements for all five attributes $(\mathbf{Y}=\left[Y^1,\ldots,Y^5\right])$ which represent samples from blasthole drilling. These are sampled from the ground truth block models with noise added to represent measurement error.

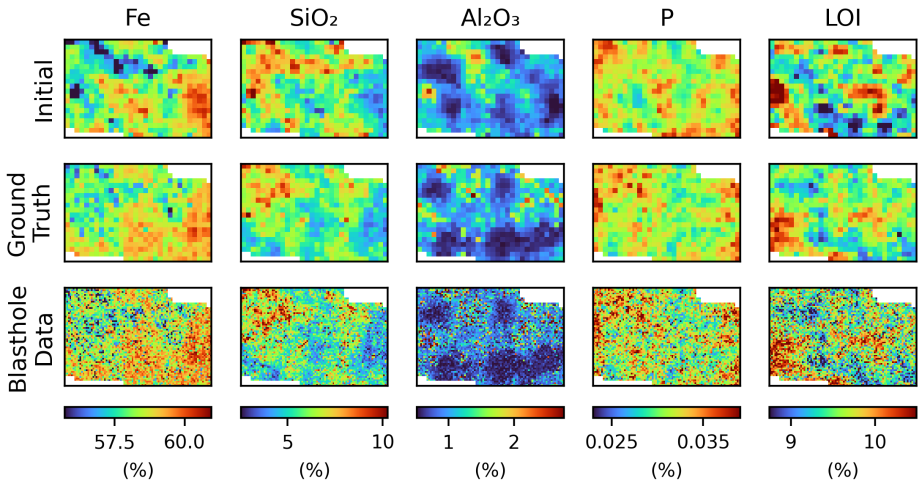

Figure 1: Selected initial simulations, ground truth models, and blasthole data for multi-attribute iron ore deposit

Two sources of processing performance measurements include (1) a contactless scanner measuring iron grade on a conveyor belt after crushing and (2) grinding mill throughput $\left(\mathbf{X}=\left[X^1,X^2\right]\right)$. These measurements are obtained for each shift in the mining sequence by identifying the blocks mined in each shift and passing their ground truth values through a hidden function. These processing performance results are allocated as block support values to the corresponding blocks to be used as conditioning data.

A mining sequence of twelve shifts is used to demonstrate the updating process. It is assumed that blocks which are mined during the shift are processed in the same shift and that no other materials (e.g. from a separate stockpile) than these blocks are processed. Each shift, the blasthole drilling measurements and the processing performance values assigned to the mined blocks are added to the

set of data used for conditioning. Figure 2 illustrates how processing performance measurements are used as block values. At the end of each shift, one round of updates is performed to all blocks which have data within a specified search distance.

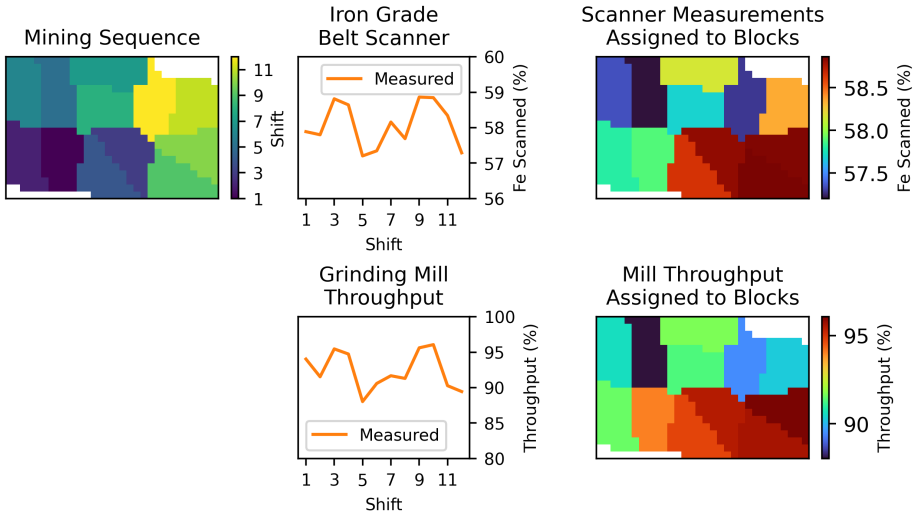

Figure 2: Mining sequence used for updating, corresponding process performance measurements, and allocation to block locations

Figure 3 shows the training images used to represent the high-order spatial statistics of the selected attributes. The TIs come from a different area of the same deposit with a dense set of blasthole data and block values. Using training images in both blasthole (point) and block support scales allows the updating approach to consider both blasthole data and surrounding block values as conditioning data. Figure 4 shows the training images with block values corresponding to both processing performance metrics, which are required for the framework to include these measurements.

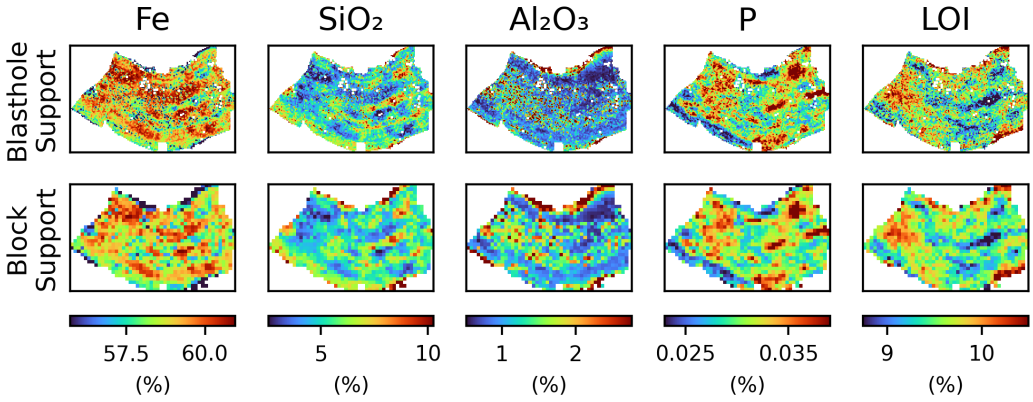

Figure 3: Training images in blasthole support and block support for the five attributes

Figure 5 displays an example realization for each attribute that has been updated using the proposed approach and the data presented. Comparing them to the initial realizations and ground truth images, the updated realizations resemble the ground truth. This suggests the updating framework is using the production data effectively, at least on a visual basis. Further validation will examine the statistical properties of the updated simulations.

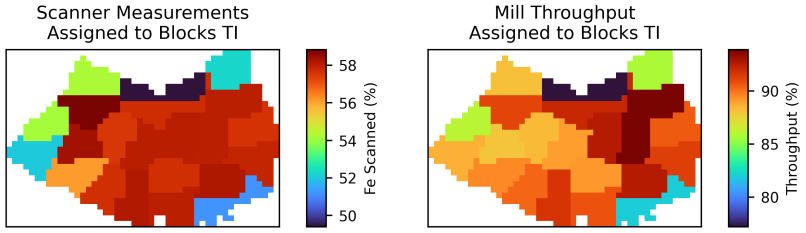

Figure 4: Training images in block support for processing performance measurements

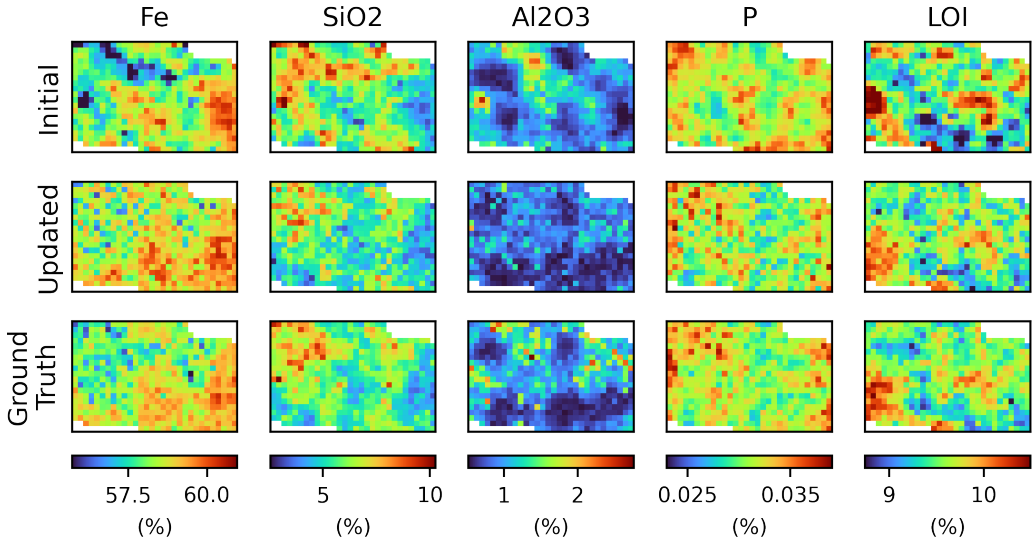

Figure 5: Selected initial and updated simulations as well as ground truth models for the five attributes

The histograms shown in Figure 6 illustrate the change in the overall distribution of the five attributes after updating. Most attributes appear to match the ground truth more closely in the updated realizations, compared to the initial realizations. It is also worth noting the distributions

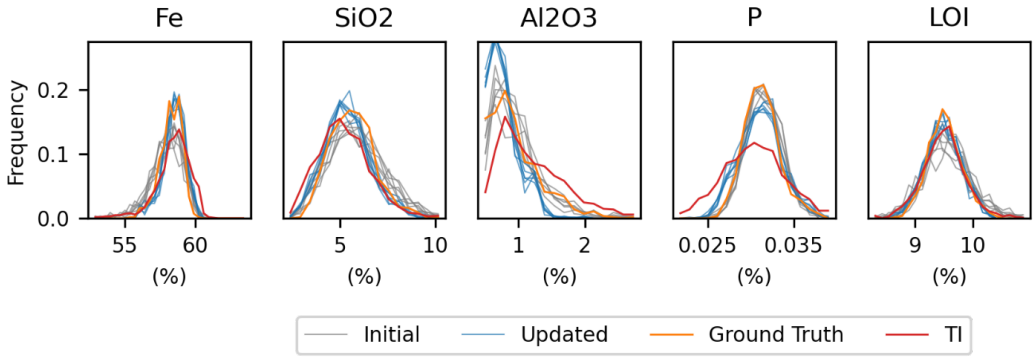

Figure 6: Histograms of ensemble simulations comparing initial, updated, ground truth, and training image

of the TIs, shown in red. Updated realizations for some attributes (e.g. iron) appear to match the ground truth despite a TI with a noticeably different distribution. However, some other attributes (e.g. phosphorus) show the opposite effect where the histograms seem to move closer to the TI and farther from the ground truth. Overall, the method shows mixed results in terms of overcoming low quality TIs.

Further validation is conducted by examining third-order spatial cumulants shown in Figure 7. These results show the spatial connectivity of grades of the ground truth image is generally well reproduced after updating in all five attributes, suggesting successful validation. In particular, the cumulant map for SiO2 appears to improve after updating. In the case of Fe and LOI, the maps from the initial simulations were already close to those of the ground truth and the updated maps maintain the same quality. The cumulant maps for most of the TIs do not appear similar to those of the ground truth models.

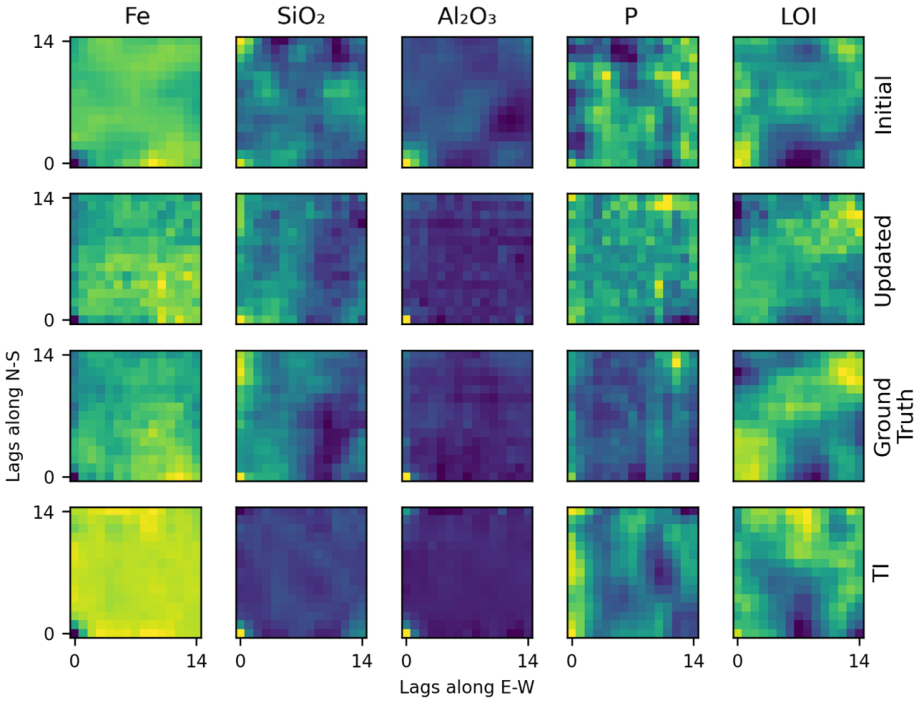

Figure 7: Third-order spatial cumulants of the initial, updated, ground truth, and training images using an L-shaped spatial template

Validation of the lag-zero correlation between the different attributes at second, third, and fourth orders is shown in Figures 8, 9, and 10, respectively. The third order (Figure 9) shows a three-dimensional array unfolded into two dimensions, with the third axis stacked vertically. The fourth order (Figure 10) continues this pattern with the third axis stacked vertically and the fourth axis stacked horizontally. At all three orders, the updated simulation appears to match the correlation patterns of the ground truth more closely than the initial simulation does. However, at all orders, the ground truth image generally shows lower correlations between different attributes than the TI or initial simulation present, potentially making it easier to reproduce.

Figure 11 shows spatial cross-cumulants which measure three-point spatial connectivity or variability between different combinations of attributes. The updated simulation shows a clear similarity to the ground truth models while the initial simulation and the TI display noticeably different patterns. Again, this highlights the method's ability to extract meaningful information from the conditioning data.

Figure 12 shows the variance at each block location in the ensemble of realizations before and after updating. The variance is not significantly lower after updating. This is an important result as there is always uncertainty present in block values despite having additional data from blastholes and processing performance. This marks an improvement over other data assimilation methods such as ensemble Kalman filter which is known to reduce variance after updating (Evensen 2003).

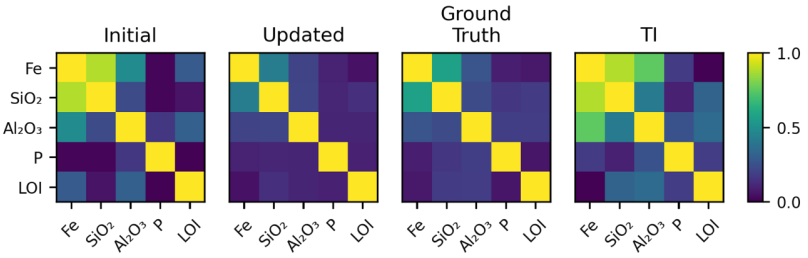

Figure 8: Covariance matrix between the five attributes for the selected initial and updated simulation, ground truth model, and training image

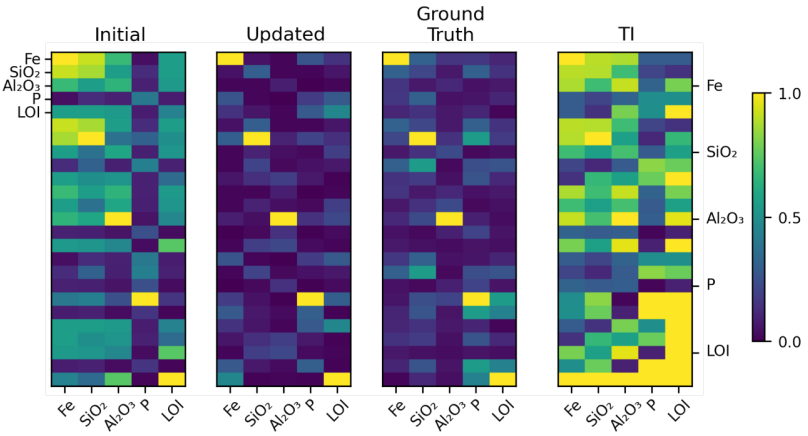

Figure 9: Third-order cross-cumulants between the five attributes for the selected initial and updated simulation, ground truth model, and training image

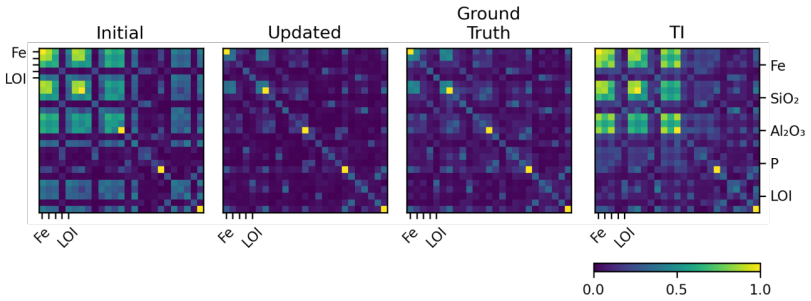

Figure 10: Fourth-order cross-cumulants between the five attributes for the selected initial and updated simulation, ground truth model, and training image

Figure 13 illustrates how the processing performance forecast and associated risk profile changes after updating the orebody simulations. The forecasts are made using a prediction model that is not connected to the updating process. There is a clear improvement in accuracy after updating as the measurements observed are much closer to the updated forecast than the initial. This improvement is quantified on the bar graph of Figure 13 which displays the change after updating in root-mean-squared-error (RMSE) between the forecasts and the measured values, where negatives values for change in RMSE suggest a reduction of error.

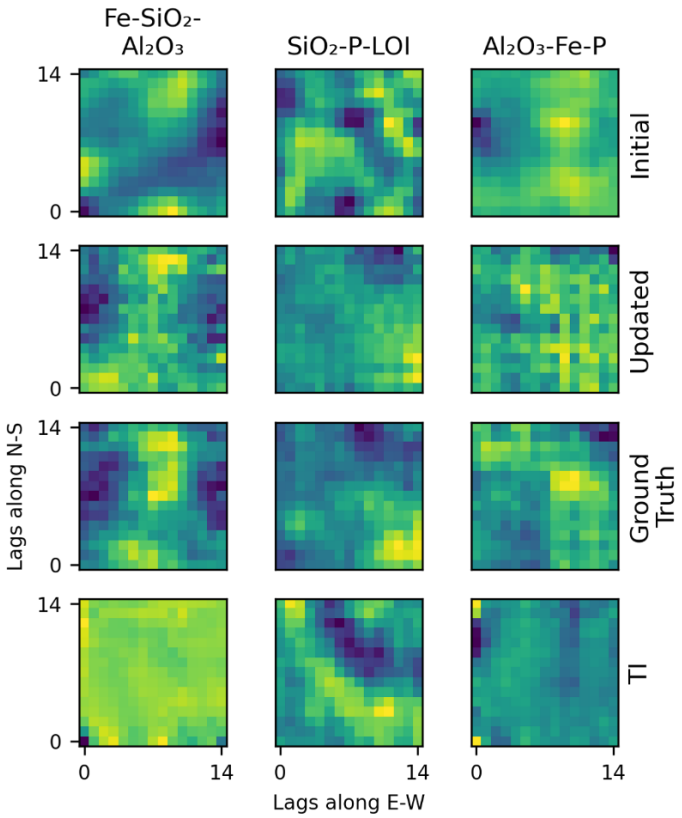

Figure 11: Third-order spatial cross-cumulants between three selected combinations for the initial and updated simulation, ground truth model, and training image using an L-shaped spatial template

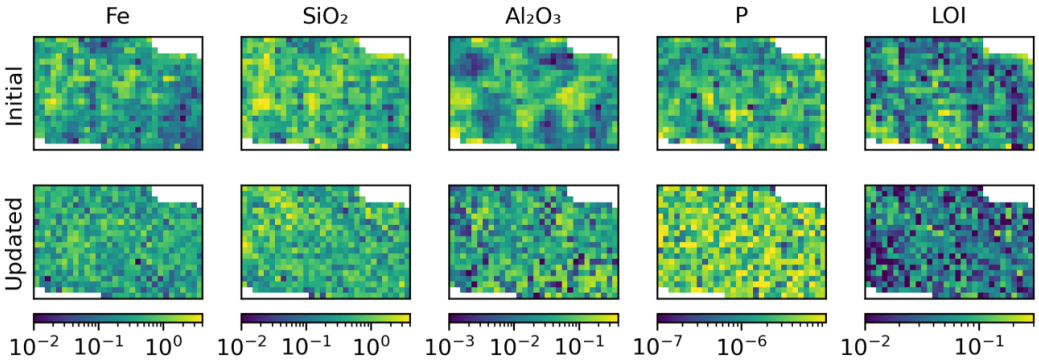

Figure 12: Variance map across ensemble of realizations for the initial and updated simulations of the five attributes

4 Conclusions

The present work proposes a framework to update multi-attribute block values from production data using high-order stochastic simulation. The framework enables the use of conditioning data of multiple support scales including point support spatial data, block values from prior realizations, and processing performance data associated with blended materials. The ability of the framework to update multiple attributes while reproducing their spatial correlations enables operations to model material properties that are critical to the quality of the final mineral products. This feature, along with the ability to use processing performance data without assuming a predefined function that connects performance to

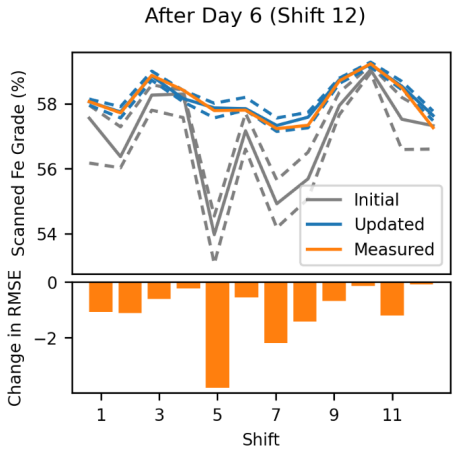

Figure 13: Processing performance forecasts from initial and updated simulations after updating with P50 shown in solid lines and P10/P90 shown in dashed lines and change in root-mean-squared-error shown as bars

block attributes, could provide value to mines with complex geometallurgical requirements. Although not every operation is able to accurately track material, this framework and further research should encourage development and adoption of material tracking tools that make data assimilation possible.

The effectiveness of the high-order updating framework is demonstrated using a multi-attribute iron ore deposit with several sources of production data. The results show that updating the simulations improves the reproduction of statistics in reference to the ground truth model, including the spatial connectivity of material properties. In addition, the updates improve the understanding of the orebody by providing more accurate forecasts for key processing performance metrics.

Being able to update processing performance forecasts enables adaptive short-term optimization of mining complexes or so-called real-time mining. Future work should build on existing optimization approaches for mine planning to capture the value provided by updating orebody simulations.

5 Appendix

The approximation coefficients used to construct a joint multivariate pdf are found in terms of the expectations of the product of the orthogonal functions

$$
\begin{aligned}
&\mathbb{E}\left[\varphi_{k_1^1}\left(z_1^1\right)\cdot\ldots\cdot\varphi_{k_{i-1}^A}\left(z_{i-1}^A\right)\cdot\varphi_{k_i^1}\left(z_i^1\right)\cdot\ldots\cdot\varphi_{k_i^a}\left(z_i^a\right)\cdot\varphi_{l_1}\left(\Lambda_1\right)\cdot\ldots\cdot\varphi_{l_{N_D}}\left(\Lambda_{N_D}\right)\right] \\
&\quad=\int_a^b\cdots\int_a^b\int_a^b\cdots\int_a^b\int_a^b\cdots\int_a^b\varphi_{k_1^1}\left(z_1^1\right)\cdot\ldots\cdot\varphi_{k_{i-1}^A}\left(z_{i-1}^A\right)\cdot\varphi_{k_i^1}\left(z_i^1\right)\cdot\ldots\cdot\varphi_{k_i^a}\left(z_i^a\right)\cdot\varphi_{l_1}\left(\Lambda_1\right)\cdot\ldots \\
&\quad\quad\cdot\varphi_{l_{N_D}}\left(\Lambda_{N_D}\right)\cdot f\left(z_1^1,b\ldots z_{i-1}^A,z_i^1,\ldots,z_i^a,\Lambda\right)\cdot dz_1^1\cdot\ldots\cdot dz_{i-1}^A\cdot dz_i^1\cdot\ldots\cdot dz_i^a \\
&\quad\quad\cdot d\Lambda_1\cdot\ldots\cdot d\Lambda_{N_D} \\
&\quad\approx\int_a^b\cdots\int_a^b\int_a^b\cdots\int_a^b\int_a^b\cdots\int_a^b\varphi_{k_1^1}\left(z_1^1\right)\cdot\ldots\cdot\varphi_{k_{i-1}^A}\left(z_{i-1}^A\right)\cdot\varphi_{k_i^1}\left(z_i^1\right)\cdot\ldots\cdot\varphi_{k_i^a}\left(z_i^a\right)\cdot\varphi_{l_1}\left(\Lambda_1\right)\cdot\ldots \\
&\quad\quad\cdot\varphi_{l_{N_D}}\left(\Lambda_{N_D}\right) \\
&\quad\quad\cdot\sum_{m_1^1=0}^{\omega}\cdots\sum_{m_{i-1}^A=0}^{\omega}\sum_{m_i^1=0}^{\omega}\cdots\sum_{m_i^a=0}^{\omega}\sum_{\lambda_1=0}^{\omega}\cdots\sum_{\lambda_{N_D}=0}^{\omega}\Big[L_{m_1^1,\ldots,m_{i-1}^A,m_i^1,\ldots,m_i^a,\lambda_1,\ldots,\lambda_{N_D}} \\
&\quad\quad\cdot\varphi_{m_1^1}\left(z_1^1\right)\cdot\ldots\cdot\varphi_{m_{i-1}^A}\left(z_{i-1}^A\right)\cdot\varphi_{m_i^1}\left(z_i^1\right)\cdot\ldots\cdot\varphi_{m_i^a}\left(z_i^a\right)\cdot\varphi_{\lambda_1}\left(\Lambda_1\right)\cdot\ldots \\
&\quad\quad\cdot\varphi_{\lambda_{N_D}}\left(\Lambda_{N_D}\right)\Big]\cdot\cdot dz_1^1\cdot\ldots\cdot dz_{i-1}^A\cdot dz_i^1\cdot\ldots\cdot dz_i^a\cdot d\Lambda_1\cdot\ldots\cdot d\Lambda_{N_D}
\end{aligned}
$$

$$
\begin{aligned}
&= \sum_{m_1^1=0}^{\omega} \cdots \sum_{m_{i-1}^A=0}^{\omega} \sum_{m_i^1=0}^{\omega} \cdots \sum_{m_i^a=0}^{\omega} \sum_{\lambda_1=0}^{\omega} \cdots \sum_{\lambda_{N_D}=0}^{\omega} \Big[L_{m_1^1,\ldots,m_{i-1}^A,m_i^1,\ldots,m_i^a,\lambda_1,\ldots,\lambda_{N_D}} \\
&\cdot \int_a^b \cdots \int_a^b \int_a^b \cdots \int_a^b \int_a^b \cdots \int_a^b \varphi_{k_1^1}\left(z_1^1\right) \cdot \varphi_{m_1^1}\left(z_1^1\right) \cdot \ldots \cdot \varphi_{k_{i-1}^A}\left(z_{i-1}^A\right) \cdot \varphi_{m_{i-1}^A}\left(z_{i-1}^A\right) \\
&\cdot \varphi_{k_i^1}\left(z_i^1\right) \cdot \varphi_{m_i^1}\left(z_i^1\right) \cdot \ldots \cdot \varphi_{k_i^a}\left(z_i^a\right) \cdot \varphi_{m_i^a}\left(z_i^a\right) \cdot \varphi_{l_1}\left(\Lambda_1\right) \cdot \varphi_{\lambda_1}\left(\Lambda_1\right) \cdot \ldots \\
&\cdot \varphi_{l_{N_D}}\left(\Lambda_{N_D}\right) \cdot \varphi_{\lambda_{N_D}}\left(\Lambda_{N_D}\right) \cdot dz_1^1 \cdot \ldots \cdot dz_{i-1}^A \cdot dz_i^1 \cdot \ldots \cdot dz_i^a \cdot d\Lambda_1 \cdot \ldots \\
&\cdot d\Lambda_{N_D} \Big] \\
&= \sum_{m_1^1=0}^{\omega} \cdots \sum_{m_{i-1}^A=0}^{\omega} \sum_{m_i^1=0}^{\omega} \cdots \sum_{m_i^a=0}^{\omega} \sum_{\lambda_1=0}^{\omega} \cdots \sum_{\lambda_{N_D}=0}^{\omega} \Big[L_{m_1^1,\ldots,m_{i-1}^A,m_i^1,\ldots,m_i^a,\lambda_1,\ldots,\lambda_{N_D}} \cdot \delta_{k_1^1 m_1^1} \cdot \ldots \\
&\cdot \delta_{k_{i-1}^A m_{i-1}^A} \cdot \delta_{k_i^1 m_i^1} \cdot \ldots \cdot \delta_{k_i^a m_i^a} \cdot \delta_{l_1 \lambda_1} \cdot \ldots \cdot \delta_{l_{N_D} \lambda_{N_D}} \Big] \\
&= L_{k_1^1,\ldots,k_{i-1}^A,k_i^1,\ldots,k_i^a,l_1,\ldots,l_{N_D}}.
\end{aligned}
$$

6 References

Benndorf J. (2015) Making use of online production data: sequential updating of mineral resource models. Mathematical Geosciences. 47, 547–563

Benndorf J. (2020) Closed loop management in mineral resource extraction: turning online geo-data into mining intelligence. Springer Nature

Both C., Dimitrakopoulos R. (2022) Integrating geometallurgical ball mill throughput predictions into short-term stochastic production scheduling in mining complexes. International Journal of Mining Science and Technology. https://doi.org/10.1016/j.ijmst.2022.10.001

Both C., Dimitrakopoulos R. (2023) Utilisation of geometallurgical predictions of processing plant reagents and consumables for production scheduling under uncertainty. International Journal of Mining, Reclamation and Environment. 37, 21–42. https://doi.org/10.1080/17480930.2022.2139350

de Carvalho J.P., Dimitrakopoulos R. (2023) Integrating short-term stochastic production planning updating with mining fleet management in industrial mining complexes: an actor-critic reinforcement learning approach. Appl Intell. 53, 23179–23202. https://doi.org/10.1007/s10489-023-04774-3

de Carvalho J.P., Dimitrakopoulos R., Minniakhmetov I. (2019) High-order block support spatial simulation method and its application at a gold deposit. Mathematical Geosciences. 51, 793–810

Chaowasakoo P., Leelasukseree C., Wongsurawat W. (2014) Introducing GPS in fleet management of a mine: Impact on hauling cycle time and hauling capacity. International Journal of Technology Intelligence and Planning. 10, 49–66

Dimitrakopoulos R., Farrelly C.T., Godoy M. (2002) Moving forward from traditional optimization: grade uncertainty and risk effects in open-pit design. Mining Technology. 111, 82–88. https://doi.org/ 10.1179/mnt.2002.111.1.82

Dimitrakopoulos R., Lamghari A. (2022) Simultaneous stochastic optimization of mining complexes - mineral value chains: an overview of concepts, examples and comparisons. International Journal of Mining, Reclamation and Environment. 36, 443–460. https://doi.org/10.1080/17480930.2022.2065730

Dimitrakopoulos R., Mustapha H., Gloaguen E. (2010) High-order Statistics of Spatial Random Fields: Exploring Spatial Cumulants for Modeling Complex Non-Gaussian and Non-linear Phenomena. Math Geosci. 42, 65–99. https://doi.org/10.1007/s11004-009-9258-9

Dimitrakopoulos R., Yao L. (2022) High-order spatial stochastic models. In: Daya Sagar, B.S., Cheng, Q., McKinley, J., and Agterberg, F. (eds.) Encyclopedia of Mathematical Geosciences. pp. 605–613. Springer, Cham, Switzerland

Dowd P. (1997) Risk in minerals projects: analysis, perception and management. Transactions of the Institutions of Mining and Metallurgy Section A-Mining Technology. 106, A9–A18

Evensen G. (1994) Sequential data assimilation with a nonlinear quasi-geostrophic model using Monte Carlo methods to forecast error statistics. Journal of Geophysical Research: Oceans. 99, 10143–10162

Evensen G. (2003) The Ensemble Kalman Filter: theoretical formulation and practical implementation. Ocean Dynamics. 53, 343–367. https://doi.org/10.1007/s10236-003-0036-9

Goodfellow R., Dimitrakopoulos R. (2016) Global optimization of open pit mining complexes with uncertainty. Applied Soft Computing. 40, 292–304. https://doi.org/10.1016/j.asoc.2015.11.038

Goodfellow R., Dimitrakopoulos R. (2017) Simultaneous stochastic optimization of mining complexes and mineral value chains. Mathematical Geosciences. 49, 341–360

Jewbali A., Dimitrakopoulos R. (2011) Implementation of conditional simulation by successive residuals. Computers & geosciences. 37, 129–142

Journel A. g., Alabert F. (1989) Non-Gaussian data expansion in the Earth Sciences. Terra Nova. 1, 123–134. https://doi.org/10.1111/j.1365-3121.1989.tb00344.x

Kitanidis P.K., Vomvoris E.G. (1983) A geostatistical approach to the inverse problem in groundwater modeling (steady state) and one-dimensional simulations. Water Resources Research. 19, 677–690. https://doi.org/10.1029/WR019i003p00677

Kumar A., Dimitrakopoulos R. (2022) Updating geostatistically simulated models of mineral deposits in real-time with incoming new information using actor-critic reinforcement learning. Computers & Geosciences. 158, 104962. https://doi.org/10.1016/j.cageo.2021.104962

Kumar A., Dimitrakopoulos R., Maulen M. (2020) Adaptive self-learning mechanisms for updating short-term production decisions in an industrial mining complex. Journal of Intelligent Manufacturing. 31, 1795–1811

La Rosa D., Rajavuori L., Korteniemi J., Wortley M. (2018) Geometallurgical Modelling and Ore Tracking at Kittilä Mine. In: Dimitrakopoulos, R. (ed.) Advances in Applied Strategic Mine Planning. pp. 451–463. Springer International Publishing, Cham

Minniakhmetov I., Dimitrakopoulos R. (2017) Joint high-order simulation of spatially correlated variables using high-order spatial statistics. Mathematical Geosciences. 49, 39–66

Minniakhmetov I., Dimitrakopoulos R., Godoy M. (2018) High-order spatial simulation using Legendre-like orthogonal splines. Mathematical geosciences. 50, 753–780

Montiel L., Dimitrakopoulos R. (2018) Simultaneous stochastic optimization of production scheduling at Twin Creeks Mining Complex, Nevada. Mining Engineering. 70, 48–56

Mustapha H., Dimitrakopoulos R. (2010) High-order Stochastic Simulation of Complex Spatially Distributed Natural Phenomena. Mathematical Geosciences. 42, 457–485. https://doi.org/10.1007/s11004-010-9291-8

Mustapha H., Dimitrakopoulos R. (2011) HOSIM: A high-order stochastic simulation algorithm for generating three-dimensional complex geological patterns. Computers & Geosciences. 37, 1242–1253. https://doi.org/10.1016/j.cageo.2010.09.007

Oliver D.S., Chen Y. (2011) Recent progress on reservoir history matching: a review. Computational Geosciences. 15, 185–221. https://doi.org/10.1007/s10596-010-9194-2

Robben C., Wotruba H. (2019) Sensor-based ore sorting technology in mining—past, present and future. Minerals. 9, 523

Rossi M.E., Deutsch C.V. (2014) Mineral Resource Estimation. Springer Netherlands, Dordrecht

Stuart A., Ord J.K. (2004) Distribution theory. Wiley & Sons, Chichester

Vargas-Guzmán J.A., Dimitrakopoulos R. (2002) Conditional simulation of random fields by successive residuals. Mathematical geology. 34, 597–611

Vargas-Guzmán J.A., Yeh T.-C.J. (1999) Sequential kriging and cokriging: Two powerful geostatistical approaches. Stochastic Environmental Research and Risk Assessment (SERRA). 13, 416–435. https://doi.org/10.1007/s004770050047

Vezhapparambu V.S., Eidsvik J., Ellefmo S.L. (2018) Rock classification using multivariate analysis of measurement while drilling data: Towards a better sampling strategy. Minerals. 8, 384

Wambeke T., Benndorf J. (2017) A simulation-based geostatistical approach to real-time reconciliation of the grade control model. Mathematical Geosciences. 49, 1–37

Wambeke T., Elder D., Miller A., Benndorf J., Peattie R. (2018) Real-time reconciliation of a geometallurgical model based on ball mill performance measurements–a pilot study at the Tropicana gold mine. Mining Technology. 127, 115–130

Yao L., Dimitrakopoulos R., Gamache M. (2018) A new computational model of high-order stochastic simulation based on spatial Legendre moments. Mathematical geosciences. 50, 929–960

Yüksel C., Thielemann T., Wambeke T., Benndorf J. (2016) Real-time resource model updating for improved coal quality control using online data. International Journal of Coal Geology. 162, 61–73. https://doi.org/10.1016/j.coal.2016.05.014